JOURNAL OF GUIDANCE, CONTROL, AND DYNAMICS
Vol. 19, No. 3, May–June 1996

Inertial Space Optimal Trajectories of Aerial Three-Dimensional Pursuit–Evasion Differential Game

A. Segal*
Israel Aircraft Industries, Lod 70350, Israel
and
T. Miloh†
Tel-Aviv University, Tel-Aviv 69978, Israel

A new differential game of a three-dimensional encounter between a fast bank-to-turn pursuer and a highly maneuverable evader has been presented, formulated, and solved in the relative (reduced) space in earlier papers. Utilizing previous results, the optimal trajectories of this new differential game are calculated in the inertial (real) space and are presented, thus providing a better physical understanding of the pursuer's and evader's actual maneuvers.

I. Introduction

LIKE many conventional aircraft and high-speed missiles, the pursuer in this game is modeled as a fast bank-to-turn vehicle that has limited maneuverability, i.e., a minimal turning radius in his pitch plane denoted by R and a limited roll rate denoted by ω_s. It is assumed that the pursuer (P) and evader (E) have both constant speeds denoted by V_P and V_E, respectively, where $V_P > V_E$. The evader is a highly maneuverable skid-to-turn (changing direction without rolling) vehicle, and it is assumed that he can change his direction in the three-dimensional space instantaneously. The encounter between players is formulated as a zero-sum differential game of kind according to the definition of Isaacs[1] and provides a generalization of two-dimensional game versions[1–3] to realistic three-dimensional aerial combat situations.[4] The game performance index, minimized by the pursuer and maximized by the evader, is the physical separation l between the two players at the final time t_f (miss distance).

The game starts at the instant when E abruptly breaks away from a tail-chase situation toward a new direction in the three-dimensional space.

Depending on the players' speed ratio $\gamma = V_E/V_P$ and P's nondimensional roll rate ω_s (normalized with respect to his maximum available pitch rate V_P/R), and for ω_s larger than a marginal value ω_m, P's optimal trajectory consists of two- or three-stage combined maneuvers, whereas E keeps on flying in his initially selected direction. P's trajectory consists of three distinct stages only if P possesses a maximum roll rate that is higher than some critical value ω_c. In this case, P is capable of aligning his pitch plane with E's trajectory, thus steering the end game (third stage) into P's preferable pitch plane. For cases where $\omega_m < \omega_s < \omega_c$, P's trajectory consists of only two stages, and the game is terminated somewhere between his pitch and yaw planes.

If ω_s is even less than ω_m, E reaches P's yaw plane before game termination and changes his direction abruptly again, so as to fly in this plane, thus, steering the end-game into P's unfavorable yaw plane. While E changes his direction instantaneously, a discontinuity in the gradient (i.e., in the costate variables) is encountered. Nevertheless, unlike in classical optimal control, where the Hamiltonian might be discontinuous at an interior point (see Bryson and Ho,[5] p. 101), the Hamiltonian remains continuous in the present zero-sum game. In this case, a four-stage combined maneuver is performed by P.

There exists a critical capture radius ℓ_c for which the relative-space trajectories form a marginally closed-barrier surface. This ℓ_c is the minimum radius that will always permit capture and is, in fact, also the maximum miss distance that E can guarantee. The game is terminated when the instantaneous separation P–E decreases and reaches ℓ_c. The different types of possible termination, i.e., classical, equilibrium, and pseudoequilibrium, that depend on the combination of γ and ω_s are introduced and described in the three earlier papers.[6–8]

This paper utilizes the relative (reduced) space solution given in Refs. 6–8 to derive the optimal time histories in the inertial (real) space for P and E separately, thus providing a better understanding of the players' actual maneuvers and trajectories in the real space. The inertial space geometry and the equations of motion are presented in Sec. II. Fortunately, the differential equations can be solved analytically yielding closed-form expressions for the direction cosines and the optimal trajectories for both the pursuer and the evader. These analytical expressions are established in Sec. III. The two-, three-, and four-stage trajectories are treated in Sec. IV. Concluding remarks are made in Sec. V.

II. Inertial Space Geometry and Equations of Motion

Figure 1 depicts the inertial frame, P's body-fixed frame and the P–E relative geometry. As a reference frame we employ the inertial frame (x_i, y_i, z_i) and transform to it the velocity vectors of P and E from the P's body-fixed frame (x_b, y_b, z_b) by utilizing the geometry of Ref. 7. P's velocity vector in his body-fixed frame is

$$V_{P_b} = V_P[1,\ 0,\ 0]^T \tag{1}$$

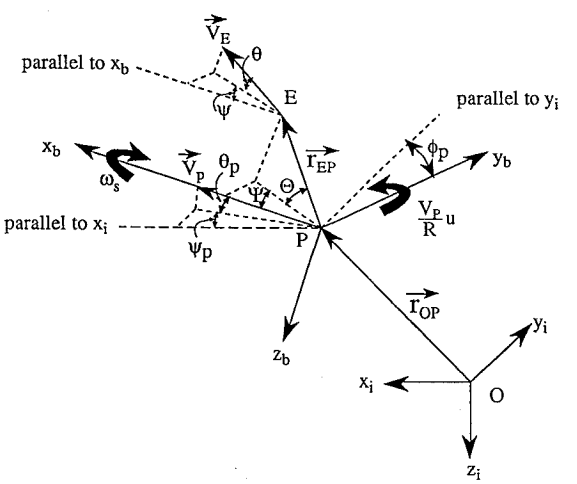

Fig. 1 Inertial and relative frame geometry and state variables.

Received Feb. 27, 1995; revision received Sept. 12, 1995; accepted for publication Nov. 20, 1995.

*G&C Project Manager.

†Professor, School of Engineering.

where T denotes the transpose of a matrix, and $V_P = |\boldsymbol{V}_{P_b}|$. E's velocity vector resolved in P's body-fixed frame is given by

$$\boldsymbol{V}_{E_b} = V_E[\cos\theta\cos\psi, \cos\theta\sin\psi, -\sin\theta]^T \tag{2}$$

where $V_E = |\boldsymbol{V}_{E_b}|$, and θ, ψ are the two heading controls of E relative to P's body axes.

E's optimal controls satisfy[7,8]

$$\cos\theta\cos\psi = \lambda_x, \qquad \cos\theta\sin\psi = \lambda_y, \qquad -\sin\theta = \lambda_z \tag{3}$$

where $\lambda_x, \lambda_y, \lambda_z$ are the components of the unit cost gradient (or the so-called costate variables) in P's body-fixed frame. P's optimal controls satisfy

$$\begin{aligned} u &= \operatorname{sgn}(\lambda_x z - \lambda_z x) = \operatorname{sgn}(s_1) \\ \omega_s &= \omega_{s_{\max}} \operatorname{sgn}(\lambda_z y - \lambda_y z) = \omega_{s_{\max}} \operatorname{sgn}(s_2) \end{aligned} \tag{4}$$

where x, y, z are the components of $\boldsymbol{r}_{EP}$ in P's body-fixed frame (see Fig. 1) and s_1 and s_2 denote the respective switching functions.

The transformation matrix from body to inertial frame is

$$[C]_b^i = [C_{ij}] \tag{5}$$

where the matrix elements C_{ij} are the nine direction cosines of P (see Ref. 9, Chap. 4). P's velocity vector transformed to the inertial frame is, thus,

$$\boldsymbol{V}_{P_i} = [C]_b^i \boldsymbol{V}_{P_b} = V_P[C_{11}, C_{21}, C_{31}]^T \tag{6}$$

where $\boldsymbol{V}_{P_b}$ is defined by Eq. (1). E's velocity vector transformed to the inertial frame is

$$\boldsymbol{V}_{E_i} = [C]_b^i \boldsymbol{V}_{E_b} = V_E[C]_b^i[\lambda_x, \lambda_y, \lambda_z]^T \tag{7}$$

where $\boldsymbol{V}_{E_b}$ is defined by Eq. (2), replacing E's controls by the optimal controls defined by Eq. (3).

Equation (7) can be rewritten in terms of E's direction cosines as follows:

$$\boldsymbol{V}_{E_i} = V_E[D_{11}, D_{21}, D_{31}]^T \tag{8}$$

where, as a result of Eq. (7), the three direction cosines of E satisfy the following relations:

$$D_{j1} = C_{j1}\lambda_x + C_{j2}\lambda_y + C_{j3}\lambda_z; \qquad j = 1, 2, 3 \tag{9}$$

Following Refs. 7 and 8, we prefer to use here the dimensionless representation of game variables and parameters in which distances are normalized with respect to R, speeds with respect to V_P, angular rates with respect to V_P/R, and time with respect to R/V_P. According to these, the scalar V_P should be omitted in Eqs. (1) and (6); the scalar V_E should be replaced by $\gamma (\gamma = V_E/V_P)$ in Eqs. (2), (7), and (8); P's pitch-rate should be represented by the nondimensional parameter u; and his roll rate ω_s should be normalized with respect to his maximum available pitch rate V_P/R.

Using the kinematic relations between direction cosines and angular rates (according to Ref. 9, Chap. 4), one gets the following differential equations for P's direction cosines:

$$\begin{aligned} \dot{C}_{j1} &= -C_{j3}u, \qquad \dot{C}_{j2} = C_{j3}\omega_s \\ \dot{C}_{j3} &= C_{j1}u - C_{j2}\omega_s; \qquad j = 1, 2, 3 \end{aligned} \tag{10}$$

To change his spatial direction, P performs a bank-to-turn maneuver, i.e., combined pitch rate and roll rate, while keeping a zero yaw rate. P's total nondimensional rate of turn is thus given by

$$\omega = \sqrt{u^2 + \omega_s^2} \tag{11}$$

We notice that Eq. (10) is very similar to the adjoint equations in Ref. 7, repeated here:

$$\dot{\lambda}_x = -u\lambda_z, \qquad \dot{\lambda}_y = \omega_s\lambda_z, \qquad \dot{\lambda}_z = u\lambda_x - \omega_s\lambda_y \tag{12}$$

Taking the derivatives of D_{j1} in Eq. (9), i.e.,

$$\dot{D}_{j1} = \sum_{i=1}^{3} \dot{C}_{ji}\lambda_i + \sum_{i=1}^{3} C_{ji}\dot{\lambda}_i; \qquad j = 1, 2, 3 \tag{13}$$

where the x, y, z subscripts of λ are replaced by $1, 2, 3$, respectively, and substituting Eq. (10) for $\dot{C}_{ji}$ and Eq. (12) for $\dot{\lambda}_i$, we readily get the following important result:

$$\dot{D}_{j1} = 0; \qquad j = 1, 2, 3 \tag{14}$$

which means that E's direction cosines are constant; therefore, E flies along straight lines in the three-dimensional space!

Based on Ref. 9, E's yaw and pitch angles relative to the inertial frame are, respectively,

$$\psi_E = \tan^{-1}(D_{21}/D_{11}), \qquad \theta_E = -\sin^{-1}D_{31} \tag{15}$$

and P's yaw, pitch, and roll angles relative to the inertial frame are, respectively,

$$\begin{aligned} \psi_P &= \tan^{-1}(C_{21}/C_{11}), \qquad \theta_P = -\sin^{-1}C_{31} \\ \phi_P &= \tan^{-1}(C_{32}/C_{33}) \end{aligned} \tag{16}$$

But unlike E's constant Euler angles defined by Eq. (15), P's [defined by Eq. (16)] are, in general, time dependent, varying along the trajectory.

The equations of motion relative to the inertial frame, based on Eqs. (6) and (8), can be simply written as

$$\dot{x}_P = C_{11}, \qquad \dot{y}_P = C_{21}, \qquad \dot{z}_P = C_{31} \tag{17}$$

where x_P, y_P, z_P are the nondimensional components of P's position vector $\boldsymbol{r}_{OP}$ (see Fig. 1), and his direction cosines C_{ji} are obtained by direct integration of Eq. (10). A similar set of equations is available for the evader:

$$\dot{x}_E = \gamma D_{11}, \qquad \dot{y}_E = \gamma D_{21}, \qquad \dot{z}_E = \gamma D_{31} \tag{18}$$

where x_E, y_E, z_E are the nondimensional components of E's position vector $\boldsymbol{r}_{OE}$, which connects O to E, i.e.,

$$\boldsymbol{r}_{OE} = \boldsymbol{r}_{OP} + \boldsymbol{r}_{EP} \tag{19}$$

and γ is E's nondimensional speed ($\gamma = V_E/V_P$).

III. Analytic Solution for Direction Cosines and Trajectories

In view of the optimality conditions (4), the set of differential equations (10) is transformed into a set of nine linear differential equations, the solution of which may be expressed as

$$\begin{aligned} C_{j1} &= -(u/\omega)a_j\cos\omega t - (u/\omega)b_j\sin\omega t \\ &\quad + (\omega_s/\omega)c_j; \qquad j = 1, 2, 3 \\ C_{j2} &= (\omega_s/\omega)a_j\cos\omega t + (\omega_s/\omega)b_j\sin\omega t \\ &\quad + (u/\omega)c_j; \qquad j = 1, 2, 3 \\ C_{j3} &= -a_j\sin\omega t + b_j\cos\omega t; \qquad j = 1, 2, 3 \end{aligned} \tag{20}$$

where ω denotes P's total nondimensional rate of turn defined by Eq. (11); $(a_j, b_j, c_j;\ j = 1, 2, 3)$ are nine initial condition (IC) constants; and C_{ji} are P's direction cosines as functions of the nondimensional time t (normalized with respect to R/V_P).

Given the IC values for C_{ji}, the nine IC constants $(a_j, b_j, c_j;\ j = 1, 2, 3)$ can be readily found. P's optimal trajectory is obtained by integrating Eq. (17), i.e.,

$$\xi_{Pj} = (\xi_{Pj})_{\mathrm{IC}} + \int_0^t C_{j1}\,d\tau; \qquad j = 1, 2, 3 \tag{21}$$

where ξ_{Pj} stands for x_P, y_P, z_P with $j = 1, 2, 3$, respectively. Using (20), we obtain

$$\begin{aligned} \xi_{Pj} &= (\xi_{Pj})_{\mathrm{IC}} - (u/\omega^2)a_j\sin\omega t - (u/\omega^2)b_j(1 - \cos\omega t) \\ &\quad + (\omega_s/\omega)c_j t; \qquad j = 1, 2, 3 \end{aligned} \tag{22}$$

Since E's direction cosines D_{ji} are constants, the prescribed IC values for D_{j1}, using Eq. (18), give E's optimal trajectory,

$$\xi_{Ej} = (\xi_{Ej})_{\mathrm{IC}} + \gamma(D_{j1})_{\mathrm{IC}}\,t; \qquad j = 1, 2, 3 \tag{23}$$

where ξ_{Ej} stands for x_E, y_E, z_E. E's Euler angles are thus defined by Eq. (15), after replacing D_{j1} by the proper initial values $(D_{j1})_{IC}$.

IV. Two-, Three-, and Four-Stage Trajectories

P's position and orientation at $t = 0$, relative to the inertial frame, may be chosen arbitrarily. A convenient choice is

$$(\boldsymbol{r}_{OP})_{IC} = \mathbf{0} \tag{24}$$

$$(\psi_P)_{IC} = (\theta_P)_{IC} = (\phi_P)_{IC} = 0 \tag{25}$$

which means that at $t = 0$ P's body-fixed frame coincides with the inertial frame (see Fig. 1).

We assume that the game starts from a tail-chase situation, where E is just ahead of P with an initial separation of x_1. Thus, according to Eqs. (19) and (24),

$$(\boldsymbol{r}_{OE})_{IC} = (\boldsymbol{r}_{EP})_{IC} = [x_1, 0, 0]^T \tag{26}$$

while the initial line-of-sight (LOS) angles are (see Fig. 1)

$$(\Psi)_{IC} = (\Theta)_{IC} = 0 \tag{27}$$

According to Eq. (25) and Ref. 9,

$$[C_{ij}]_{IC} = [I] \tag{28}$$

where $[I]$ denotes the 3×3 identity matrix.

The initial optimal gradient in P's body axes is[7]

$$[\lambda_x, \lambda_y, \lambda_z]_{IC} = \left[0, \pm\sqrt{1 - (\gamma/x_1)^2}, \pm\gamma/x_1\right] \tag{29}$$

which may be transformed to the inertial frame by using Eqs. (9) and (28). An immediate conclusion is that the components of the gradient in the inertial frame, which are actually three of E's constant direction cosines, coincide with the respective gradient components in P's body axes at $t = 0$, i.e.,

$$\begin{aligned} D_{11} &= \cos\theta_E \cos\psi_E = 0 \\ D_{21} &= \cos\theta_E \sin\psi_E = \pm\sqrt{1 - (\gamma/x_1)^2} \\ D_{31} &= -\sin\theta_E = \pm\gamma/x_1 \end{aligned} \tag{30}$$

(see also Ref. 9).

Except from the limiting case of $\omega_s \to \infty$, for which the present differential game degenerates into the familiar Homicidal Chauffeur[1,2] game where $x_1 = \gamma$, we have $x_1 > \gamma$ (see Fig. 8 of Ref. 7) for all optimal closed-barrier trajectories. Thus, according to Eq. (30), E's Euler angles must satisfy

$$\psi_E = \pm\pi/2, \qquad \theta_E = \pm\sin^{-1}(\gamma/x_1) \tag{31}$$

The $\pm$ signs in Eqs. (29–31) indicate that the point $(x_1, 0, 0)$ is in fact an efferent (or dispersal) point[1] that defines the separation between P and E at the instant when E changes his spatial direction abruptly from a tail-chase situation to one of the four new directions defined by Eq. (31). The reader is reminded that our game starts precisely at this point.

From Eqs. (14) and (31) we conclude that E remains in a plane that is perpendicular to the initial LOS vector $(\boldsymbol{r}_{EP})_{IC}$ [see Eq. (26)], and flies along a straight line, the slope angle of which is θ_E [see Eq. (31)]. This situation holds for $0 < t \le t_f$ as long as P's roll rate ω_s is higher than some marginal value ω_m. In the less practical case, when P is hampered by a small roll rate ($\omega_s < \omega_m$), E changes his direction instantaneously again at some $t < t_f$, when reaching P's yaw plane,[7] and then flies along a new line in the three-dimensional space [satisfying Eq. (14)] until termination at $t = t_f$.

Without a loss of generality, we consider here only one of E's possible choices defined by Eq. (31), which is the abrupt yaw-right, pitch-down turn, i.e.,

$$\psi_E = +\pi/2, \qquad \theta_E = -\sin^{-1}(\gamma/x_1) \tag{32}$$

(the other three possible choices lead to similar trajectories for E and P).

A. Two-Stage Trajectory

If P's roll-rate ω_s is higher than a marginal value ω_m but still lower than a critical value ω_c, where ω_m and ω_c depend on the speed ratio γ, then P's optimal trajectory consists of two stages. It is shown in Refs. 7 and 8 that for E's choosing Eq. (32) at $t = 0^+$, P's optimal controls are given by $u = -1$ and $\omega_s = +\omega_{s_{max}}$.

Using Eq. (28) along with P's optimal controls, one gets the nine IC constants, $(a_j, b_j, c_j;\ j = 1, 2, 3)$. Using Eq. (20), along with the IC constants the direction cosine matrix is obtained.

According to Eqs. (22), (24), and the corresponding IC constants, the first stage of P's optimal trajectory is given by the position vector, the components of which are

$$\begin{aligned} x_P &= (1/\omega^3)\sin\omega t + \left(\omega_s^2/\omega^2\right)t \\ y_P &= \left(\omega_s/\omega^3\right)\sin\omega t - \left(\omega_s/\omega^2\right)t \\ z_P &= (1/\omega^2)(1 - \cos\omega t) \end{aligned} \tag{33}$$

Equation (33) holds only for

$$0 \le t \le t_{s_1} \tag{34}$$

where t_{s_1} is the time at which the switching function s_1 [see Eq. (4)] becomes zero. At this instant P switches his pitch-rate control u to $+1$ and starts flying along the second and final stage of his trajectory, thus approaching E in an optimal manner by applying his maximum total rate of turn in the right direction.[7,8]

Since the switching surface does not cause a discontinuity in the gradient[1,5] and since P's Euler angles are continuous (because of his limited rate of turn), we conclude, according to Eq. (9), that

$$D_{j1}\left(t_{s_1}^+\right) = D_{j1}\left(t_{s_1}^-\right); \qquad j = 1, 2, 3 \tag{35}$$

Equation (35), along with Eq. (14), indicates that E follows a straight-line course, described by

$$x_E = x_1, \qquad y_E = \gamma\sqrt{1 - (\gamma/x_1)^2}\, t, \qquad z_E = \left(\gamma^2/x_1\right)t \tag{36}$$

which results from Eqs. (23), (26), and (30). Note that E's trajectory is not affected by P's control switching and is kept by E from $t = 0$ to t_f. Let us next define the shifted time

$$t' \triangleq t - t_{s_1}; \qquad 0 < t' \le t_f - t_{s_1} \tag{37}$$

and calculate the nine new IC constants (at $t' = 0^+$). Recall that $u = +1$ for $t' > 0$.

The new IC position of P $(x_{Ps_1}, y_{Ps_1}, z_{Ps_1})$ is readily obtained from Eq. (33) by substituting $t = t_{s_1}$. Finally, the second stage of P's optimal trajectory according to Eq. (22), using the new IC position and the shifted time, is defined by

$$\begin{aligned} \xi_{Pj} = \xi_{Pjs_1} &- (1/\omega^2)a_{js_1}\sin\omega t' - (1/\omega^2)b_{js_1}(1 - \cos\omega t') \\ &+ (\omega_s/\omega)c_{js_1}t'; \qquad j = 1, 2, 3 \end{aligned} \tag{38}$$

where ξ_{Pj} represents x_P, y_P, z_P for $j = 1, 2, 3$, respectively; similarly, ξ_{Pjs_1} represents $x_{Ps_1}, y_{Ps_1}, z_{Ps_1}$, where $a_{js_1}, b_{js_1}, c_{js_1}$ $(j = 1, 2, 3)$ are the nine new IC constants, and t' is the shifted time defined by Eq. (37).

Two numerical examples, illustrated graphically, are chosen to present the two-stage trajectory, where the first example shows a classical termination and the second example presents a pseudo-equilibrium termination.[8]

Example 1: The pursuer's speed is $V_P = 1000$ m/s, the evader's speed is $V_E = 500$ m/s (i.e., $\gamma = 0.5$), the pursuer's pitch-plane minimum turning radius is $R = 573$ m (i.e., maximum pitch rate $= 100$ deg/s), and the pursuer's maximum roll rate is $\omega_{s_{max}} = 100$ deg/s (i.e., nondimensional $\omega_{s_{max}} = 1$)

The three-dimensional trajectories of P and E are projected on the z_i–x_i and y_i–x_i planes (see Fig. 2) and on the y_i–z_i plane (see Fig. 3). As in the planar case,[2] the game terminates classically with

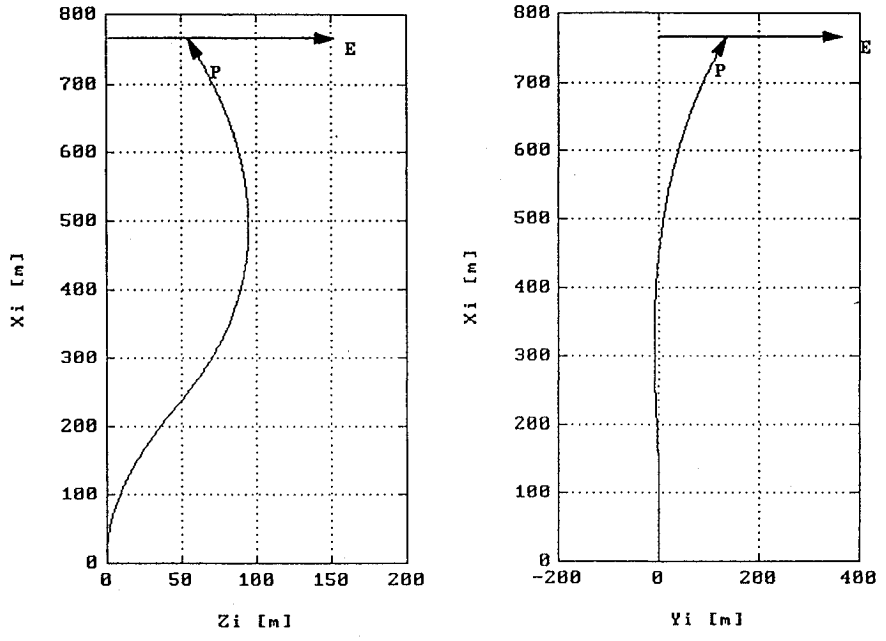

Fig. 2 Inertial space trajectory projections, example 1; V_P = 1000 m/s, V_E = 500 m/s, R = 573 m, and W_S = 100 deg/s.

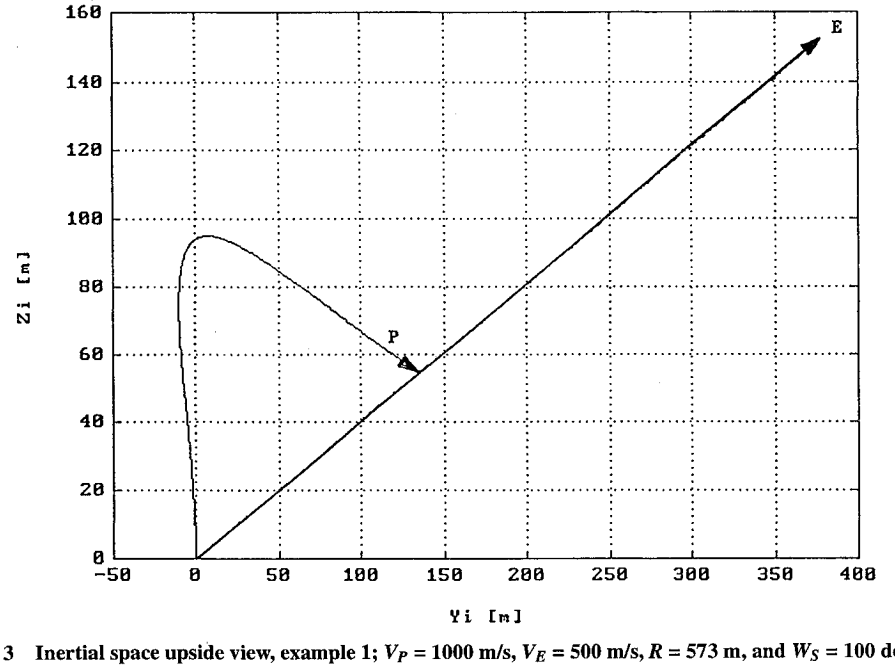

Fig. 3 Inertial space upside view, example 1; V_P = 1000 m/s, V_E = 500 m/s, R = 573 m, and W_S = 100 deg/s.

P's curved trajectory intersecting the straight line along which E flies. The distance from this intersection point to E's final position is ℓ_c, and its full size appears in Fig. 3. In Fig. 2 the projections of ℓ_c appear as $\ell_c|\sin\theta_E| = \ell_c\gamma/x_1$ on the z_i–x_i plane and $\ell_c\cos\theta_E = \ell_c\sqrt{[1-(\gamma/x_1)^2]}$ on the y_i–x_i plane [again, distances from the intersection points to E's (projected) final position].

As shown in Fig. 3, P turns away first from E, mainly toward the z_i direction, thus being able afterwards to perform a very tight three-dimensional turn toward E, using his maximum rate of turn. This maneuver is similar to the swerve maneuver in the Homicidal Chauffeur game[1] where, in some cases, P chooses this kind of maneuver to approach E within a minimum time.

Example 2: The pursuer's speed is V_P = 1000 m/s, the evader's speed is V_E = 800 m/s (γ = 0.8), the pursuer's pitch-plane minimum turning radius is R = 573 m, and the pursuer's maximum roll rate is $\omega_{s_{\max}}$ = 100 deg/s (i.e., nondimensional $\omega_{s_{\max}} = 1$).

Figure 4 presents the projections of P's and E's trajectories on the z_i–x_i and y_i–x_i planes, and Fig. 5 depicts the projections of these trajectories on the y_i–z_i plane. Similarly to the planar case,[2] for a pseudoequilibrium termination, P's trajectory does not intersect the line along which E flies, meaning that P does not reach the $x_i = x_1$ plane. The dashed lines in Figs. 4 and 5 represent projections of ℓ_c where, obviously, $\ell_c = \sqrt{[(x_{E_f}-x_{P_f})^2+(y_{E_f}-y_{P_f})^2+(z_{E_f}-z_{P_f})^2]}$.

B. Three-Stage Trajectory

If P's roll rate is higher than a critical value ω_c, P is capable of steering the end game into his favorable pitch plane. In this case, the second stage of the trajectory does not actually reach the target set, but it is rather a tributary to a ω_s—universal line (UL). The segment of this UL starts where the tributary meets the UL and terminates at the target set.[7,8] Along this segment $\omega_s = 0$ and $u = +1$.

Based on the continuity of the gradient and of P's direction cosines, we conclude again that [see Eq. (9)]

$$D_{j1}(t_B^+) = D_{j1}(t_B^-); \qquad j = 1, 2, 3 \tag{39}$$

where $t = t_B$ is the time at which the tributary meets the UL segment.

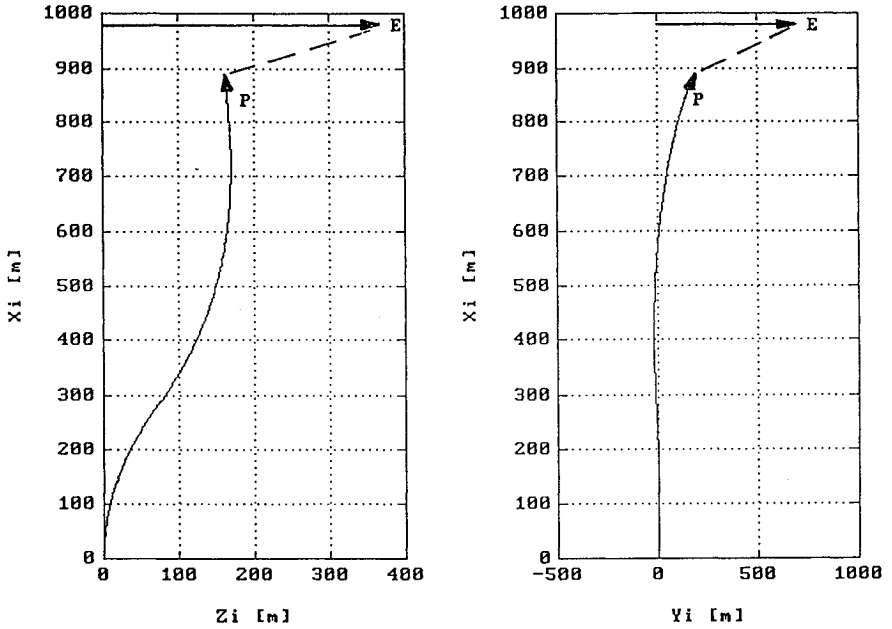

Fig. 4 Inertial space trajectory projections, example 2; V_P = 1000 m/s, V_E = 800 m/s, R = 573 m, and W_S = 100 deg/s.

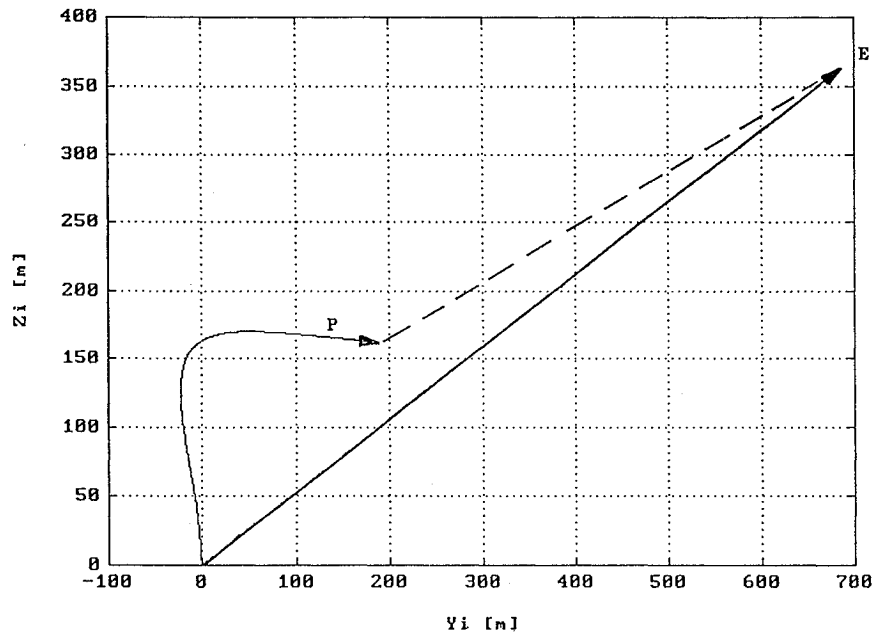

Fig. 5 Inertial space upside view, example 2; V_P = 1000 m/s, V_E = 800 m/s, R = 573 m, and W_S = 100 deg/s.

Thus, E keeps his straight line trajectory (36), satisfying Eq. (14), which is not affected by P's ω_s switching from $+\omega_{s_{\max}}$ to 0.

Next, we define a second shifted time,

$$t'' \triangleq t - t_B; \qquad 0 < t'' \leq t_f - t_B \tag{40}$$

and calculate again the nine IC constants (at $t'' = 0^+$).

The new IC position of P $(x_{P_B}, y_{P_B}, z_{P_B})$ is obtained by substituting $t' = t_B - t_{s_1}$ in Eq. (38) (in which ω_s, is still $\omega_{s_{\max}}$), getting $\xi_{P_{jB}}$; P's UL segment is defined by

$$\xi_{P_j} = \xi_{P_{jB}} + C_{j1}(t_B)\sin t'' - C_{j3}(t_B)(1 - \cos t''); \qquad j = 1, 2, 3 \tag{41}$$

where, again, ξ_{P_j} represents x_P, y_P, z_P for $j = 1, 2, 3$, respectively.

Again, two numerical examples are chosen to illustrate the three-stage trajectory, where in one example the termination is a classical one and in the other the game ends with equilibrium terminal conditions.[8]

Example 3: The pursuer's speed is $V_P = 1000$ m/s, the evader's speed is $V_E = 500$ m/s ($\gamma = 0.5$), the pursuer's pitch-plane minimum turning radius is $R = 573$ m, and the pursuer's maximum roll rate is $\omega_{s_{\max}} = 700$ deg/s (i.e., nondimensional $\omega_{s_{\max}} = 7$).

The projections of the trajectories on the z_i–x_i and y_i–x_i planes are depicted in Fig. 6, and the projection on the y_i–z_i plane is presented in Fig. 7. Each of the projections in Fig. 6 is very similar to the classical terminating planar game trajectory of Breakwell and Merz.[2] Figure 7 shows P turning away just slightly, then tightening his turn, and begin keeping E under a firm track.

In the planar game, in which P does not perform any out-of-plane maneuvers, Fig. 7 should show coinciding P's and E's trajectories, from the upside view. Actually, because of P's high roll rate in this example, his trajectory does not deviate much from E's trajectory, referring to the upside view of Fig. 7. It has been also demonstrated in Refs. 7 and 8 that by letting $\omega_{s_{\max}} \to \infty$, our three-dimensional game degenerates into the familiar Homicidal Chauffeur planar game.[1]

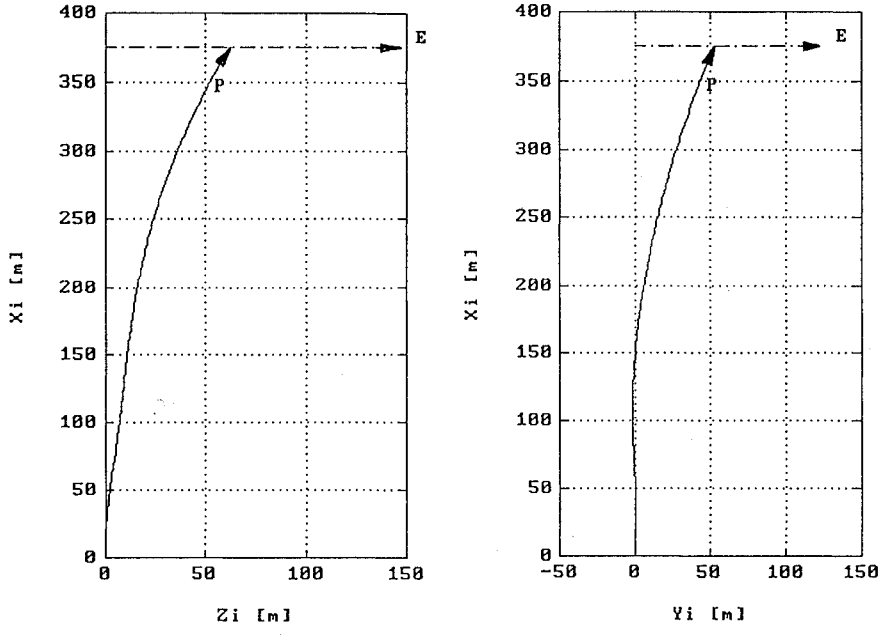

Fig. 6 Inertial space trajectory projections, example 3; V_P = 1000 m/s, V_E = 500 m/s, R = 573 m, and W_S = 700 deg/s.

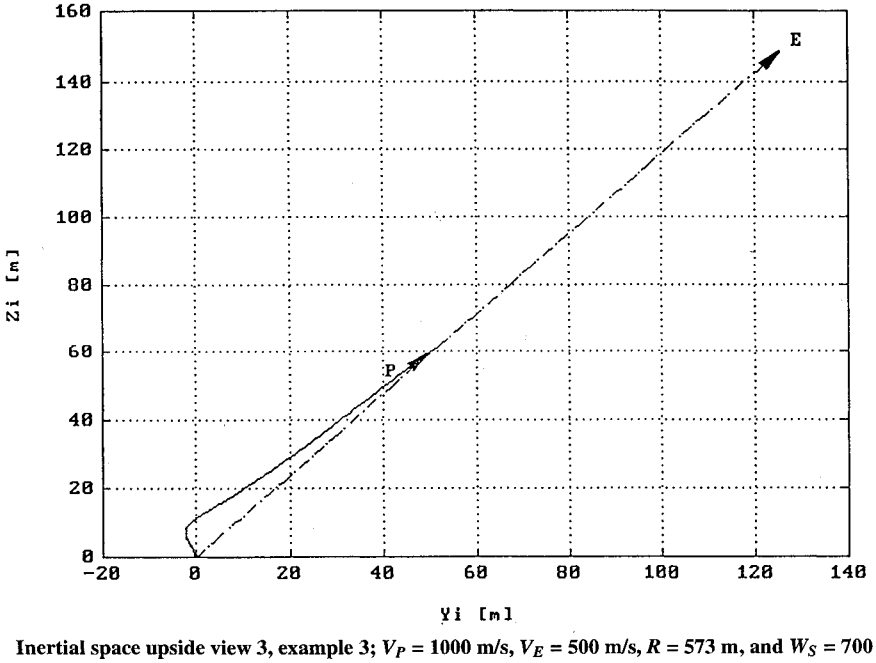

Fig. 7 Inertial space upside view 3, example 3; V_P = 1000 m/s, V_E = 500 m/s, R = 573 m, and W_S = 700 deg/s.

Example 4: The pursuer's speed is $V_P = 1000$ m/s, the evader's speed is $V_E = 900$ m/s ($\gamma = 0.9$), the pursuer's pitch-plane minimum turning radius is $R = 573$ m, and the pursuer's maximum roll rate is $\omega_{s_{\max}} = 344$ deg/s (nondimensional $\omega_{s_{\max}} = 3.44$).

The projections of P's and E's trajectories on the z_i–x_i and y_i–x_i planes are depicted in Fig. 8. The termination is, again, very similar to the equilibrium termination of the planar game.[2] The upside view of the trajectories is presented by Fig. 9. Here, P's out-of-plane maneuver is a little larger than in the preceding example; but again, the upside view deviation from E's trajectory is quite small.

C. Four-Stage Trajectory

The range in which P's roll-rate is lower than a marginal $\omega_{s_{\max}} = \omega_m$ is clearly of limited practical value. Nevertheless, the optimal trajectories in this region are interesting and instructive from the theoretical point of view. The first stage of the four-stage trajectory behaves in a similar manner to the two earlier cases (i.e., two- and three-stage trajectories), starting with $|r_{EP}| = x_1$ and terminating at the $s_1 = 0$ switching line, at which P switches his pitch-rate control from $u = -1$ to $+1$. The second stage reaches the $s_2 = 0$ switching line, at which P switches his roll-rate control from $\omega_s = +\omega_{s_{\max}}$ to $-\omega_{s_{\max}}$. The third stage, along which $u = +1$ and $\omega_s = -\omega_{s_{\max}}$, is a short-time tributary[7] that ends on P's wing plane, where E changes his direction instantaneously to steer the end game into P's unfavorable yaw plane, causing a discontinuity in the gradient. The fourth stage (the end game) continues along a segment of a (u, ω_s)–UL, along which $u = \omega_s = 0$, and reaches the target set at $t = t_f$.

Since a switching surface does not cause a discontinuity in the gradient[15] and since P's direction cosines are continuous, we conclude again that [see Eq. (9)]

$$D_{j1}\left(t_{s_2}^{+}\right) = D_{j1}\left(t_{s_2}^{-}\right); \qquad j = 1, 2, 3 \tag{42}$$

where t_{s_2} is the time at which the switching function s_2 [see Eq. (4)] becomes zero. Thus, E does not change his attitude controls, and

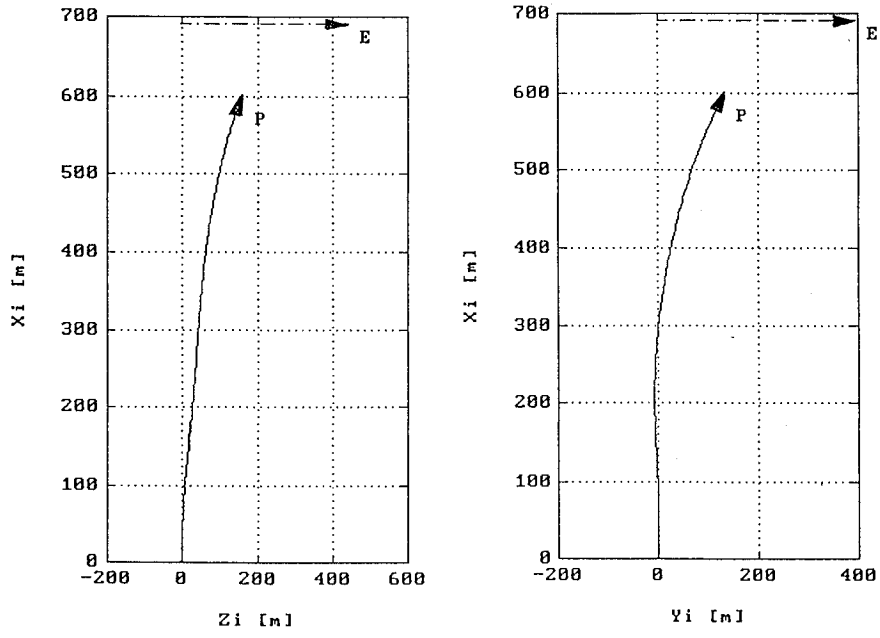

Fig. 8 Inertial space trajectory projections, example 4; V_P = 1000 m/s, V_E = 900 m/s, R = 573 m, and W_S = 344 deg/s.

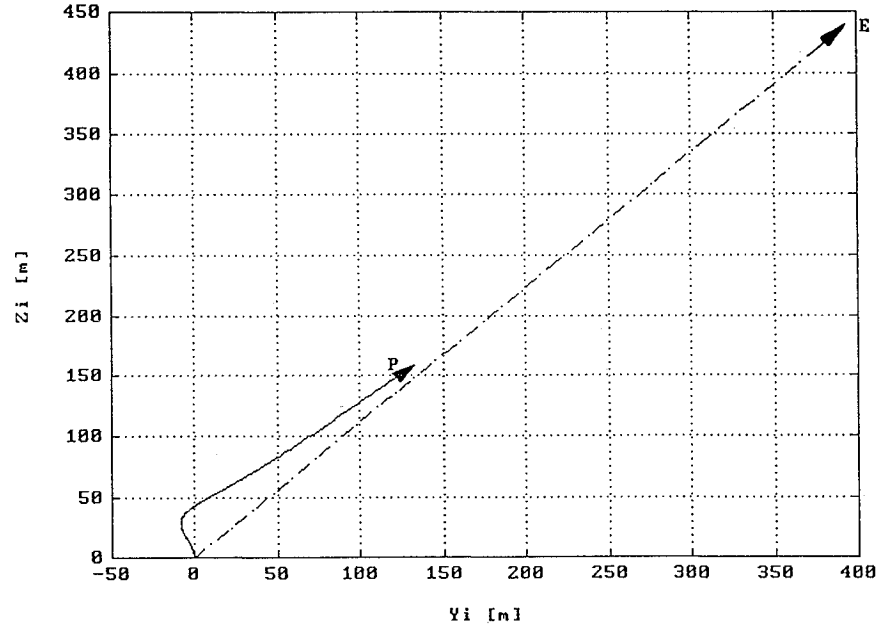

Fig. 9 Inertial space upside view, example 4; V_P = 1000 m/s, V_E = 900 m/s, R = 573 m, and W_S = 344 deg/s.

his straight line trajectory, defined by Eq. (36), is not affected by P's ω_s switching. The nine IC constants (at $t = t_{s_2}^+$) are simply obtained by using $C_{ij}(t_{s_2})$ instead of $(C_{ij})_{\text{IC}}$ along with $u = +1$ and $\omega_s = -\omega_{s_{\max}}$.

It is necessary to define now a third shifted time,

$$t''' \triangleq t - t_{s_2}; \qquad 0 < t''' \leq t_A - t_{s_2} \tag{43}$$

where t_A is the time at which E reaches P's wing plane.

Replacing the subscript s_1 by s_2 and substituting $\omega_s = -\omega_{s_{\max}}$ in Eq. (38) we get P's position as a function of t''', where t''' replaces t',

$$\xi_{Pj} = \xi_{Pjs_2} - \frac{1}{\omega^2} a_{js_2} \sin \omega t''' - \frac{1}{\omega^2} b_{js_2}(1 - \cos \omega t''')$$

$$- \frac{\omega_{s_{\max}}}{\omega} c_{js_2} t'''; \qquad j = 1, 2, 3 \tag{44}$$

Here $a_{js_2}, b_{js_2}, c_{js_2}$ $(j = 1, 2, 3)$ are the nine IC constants at $t = t_{s_2}^+$, and ξ_{Pjs_2} is the initial position at $t = t_{s_2}$.

As stated before, P's direction cosines are always continuous; therefore,

$$C_{ij}(t_A^+) = C_{ij}(t_A^-); \qquad i, j = 1, 2, 3 \tag{45}$$

while P switches his controls to $u = 0$ and $\omega_s = 0$. On the other hand, E changes his controls abruptly, while introducing a discontinuity in the gradient components

$$\lambda_x(t_A^+) \neq \lambda_x(t_A^-); \qquad \lambda_y(t_A^+) \neq \lambda_y(t_A^-)$$
$$\lambda_z(t_A^+) \neq \lambda_z(t_A^-) \tag{46}$$

and, accordingly,

$$D_{j1}(t_A^+) \neq D_{j1}(t_A^-); \qquad j = 1, 2, 3 \tag{47}$$

Along the UL segment, which starts at $t = t_A$ and ends at $t = t_f$, P's direction cosines and the gradient components all remain constants,

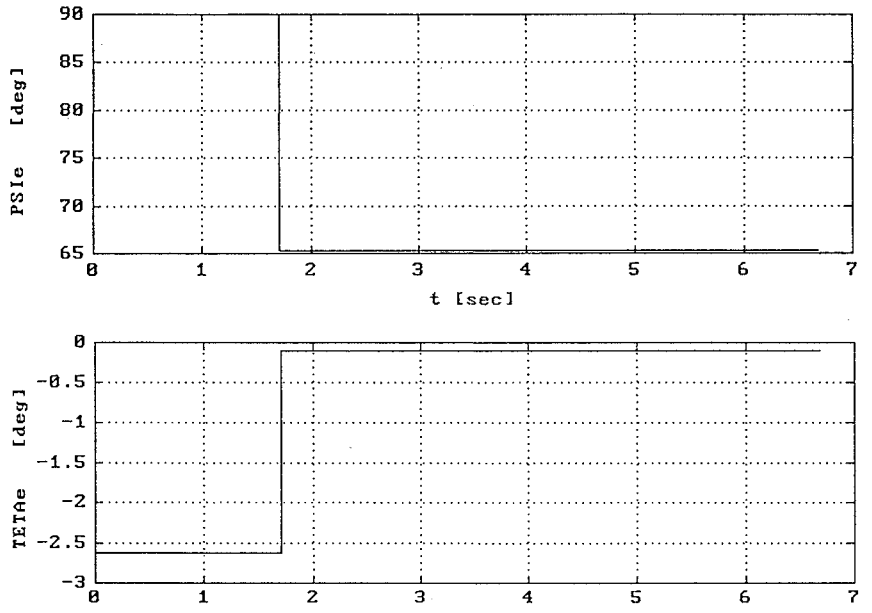

Fig. 10 Euler angles of E, example 5; V_P = 1000 m/s, V_E = 500 m/s, R = 573 m, and W_S = 5 deg/s.

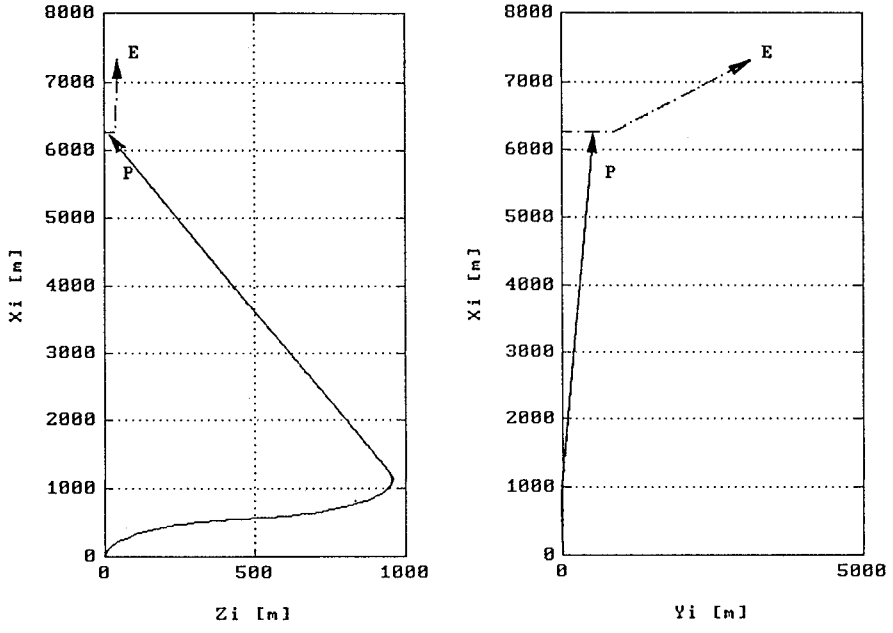

Fig. 11 Inertial space trajectory projections, example 5; V_P = 1000 m/s, V_E = 500 m/s, R = 573 m, and W_S = 5 deg/s.

which follows directly from Eqs. (10) and (12) after substituting $u = \omega_s = 0$. According to Ref. 7, for $t_A < t \leq t_f$,

$$\lambda_x = \lambda_{x_f} = \gamma; \qquad \lambda_y = \lambda_{y_f} = \sqrt{1-\gamma^2}; \qquad \lambda_z = \lambda_{z_f} = 0 \tag{48}$$

and according to Eq. (9),

$$D_{j1} = \gamma C_{j1}(t_A) + \sqrt{1-\gamma^2}\, C_{j2}(t_A); \qquad j = 1, 2, 3 \tag{49}$$

where $C_{ji}(t_A)$ are P's direction cosines at $t = t_A$. E's optimal trajectory is readily obtained from Eq. (23):

$$\xi_{Ej} = \xi_{Ej}(t_A) + \gamma D_{j1} t''''; \qquad j = 1, 2, 3 \tag{50}$$

where $\xi_{Ej}(t_A)$ are E's position vector components at $t = t_A$, the D_{j1} are defined by Eq. (49), and t'''' is yet another shifted time,

$$t'''' \triangleq t - t_A; \qquad 0 < t'''' \leq t_f - t_A \tag{51}$$

Obviously, P's trajectory along the UL is also shown to be a straight line simply defined by Eq. (21),

$$\xi_{Pj} = \xi_{Pj}(t_A) + C_{j1}(t_A) t''''; \qquad j = 1, 2, 3 \tag{52}$$

The following numerical example is chosen to illustrate and clarify the features of the four-stage trajectory.

Example 5: The pursuer's speed is $V_P = 1000$ m/s, the evader's speed is $V_E = 500$ m/s ($\gamma = 0.5$), the pursuer's pitch-plane minimum turning radius is $R = 573$ m, and the pursuer's maximum roll rate is $\omega_{s_{\max}} = 5$ deg/s (nondimensional $\omega_{s_{\max}} = 0.05$).

Figure 10 shows E's Euler angles that behave like step functions. It should be noticed that E chooses a small pitch angle θ_E right from the beginning, trying to stay as close as possible to P's yaw plane and taking advantage of P's low roll rate along with his lack of yaw-rate control (note that at $t = 0^+$: $\psi_E = 90$ deg whereas $\psi_P = 0$). In the earlier examples, where P possesses a much larger roll rate, the optimal (and constant) θ_E chosen by E is much higher, as can be concluded from Figs. 3, 5, 7, and 9, θ_E being the slope angle of E's straight line trajectories in these upside views.

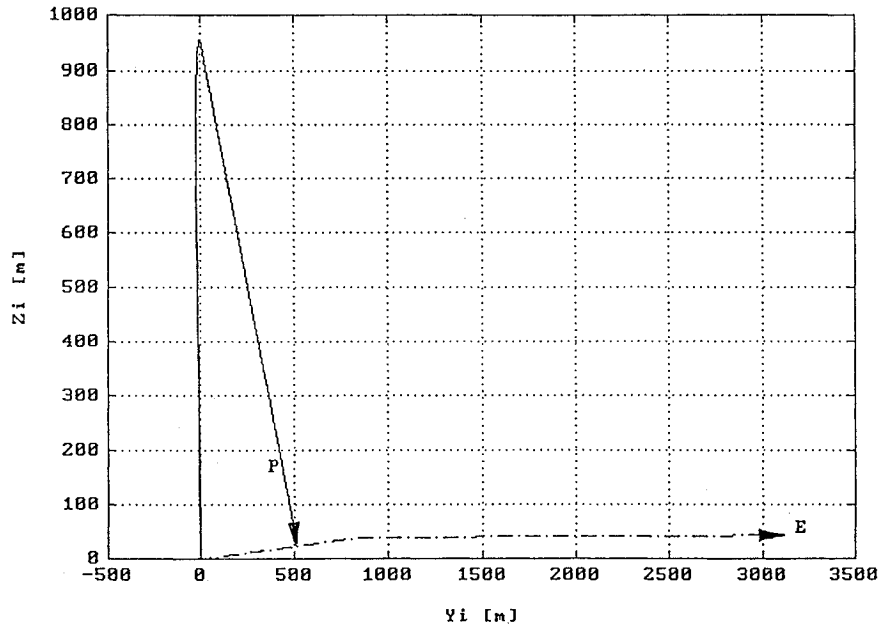

Fig. 12 Inertial space upside view, example 5; V_P = 1000 m/s, V_E = 500 m/s, R = 573 m, and W_S = 5 deg/s.

The three-dimensional trajectories are projected on the z_i–x_i and y_i–x_i planes (see Fig. 11) and on the y_i–z_i plane (see Fig. 12), indicating that in this example both P and E maneuver out-of-plane. Although the trajectories in this case are much different from all of the others mentioned before, the termination of the game is still a classical one.[7,8] Figures 11 and 12 show P's trajectory intersecting the straight line along which E originally flew (before breaking away toward his new and final direction in the three-dimensional space). P, being hampered by his relatively small roll rate, performs a very large turn out-of-plane, mainly toward the z_i direction (see Fig. 12), during which he combines his pitch and roll-rate controls to find himself, finally, turning optimally back toward E's flight path. It is clear in this example that trying to turn toward E right from the beginning will not help P much because, as stated before, E chooses to fly very close to P's yaw plane in which P does not have any maneuverability at all.

V. Concluding Remarks

As presented in earlier papers, the relative space trajectory consists of a different number of stages, depending on P's roll-rate magnitude. For a roll rate that is larger than a marginal value ω_m but less than a critical value ω_c, the trajectory consists of two stages. For a roll rate that is higher than ω_c, P's trajectory consists of three stages. If P's roll rate is less than ω_m, which is a case with limited practical value for design purposes, the trajectory consists of four stages.

It is shown that E flies along straight lines in the three-dimensional inertial space, by proving that his direction cosines are constant. The game starts from a tail-chase situation with E being just ahead of P with an initial separation x_1, where E chooses the right instant to abruptly break away. If P's roll rate is higher than ω_m, E remains in a plane that is perpendicular to the initial LOS vector. (E's choice selected in this paper is the yaw-right, pitch-down maneuver where, obviously, the three other choices lead to symmetrical trajectories.) For roll rates that are less than ω_m, E takes advantage of P's low roll rate (along with P's lack of yaw-rate control) and abruptly changes again his direction, once he reaches P's yaw plane. From this instant and thereafter, E flies along a new straight line in P's yaw plane.

In addition to the general analytical solution, five numerical examples have been chosen to demonstrate the various maneuvers executed by P and E with the different types of game termination, namely, classical, equilibrium, and pseudoequilibrium terminations.[8] The trajectories are presented graphically. Classical game termination is indicated by P's trajectory intersecting the line along which E flies. When P's trajectory does not intersect the line along which E flies (i.e., P's trajectory does not reach the $x_i = x_1$ plane), the game termination is of a pseudoequilibrium or equilibrium type. It is also demonstrated that the lower the available roll rate the more P has to swerve, resulting in large deviations from E's flight path. Comparing the five examples, the best situation for P is presented by example 3. Because of P's high roll rate and E's (relatively) low speed, here P almost does not have to perform out-of-plane (or swerve) maneuvers.

It is believed that the presentation of the various players' maneuvers and different types of trajectories in the three-dimensional inertial space, which is the scope of this paper, contributes a great deal to the better physical understanding of this novel aerial pursuit–evasion game.

References

[1]Isaacs, R., *Differential Games*, Krieger, New York, 1975.

[2]Breakwell, J. V., and Merz, A. W., "Minimum Required Capture Radius in Coplanar Model of the Aerial Combat Problem," *AIAA Journal*, Vol. 15, 1987, p. 1089–1094.

[3]Miloh, T., "The Game of Two Ellipsoidal Ships," *Optimal Control Applications and Methods*, Vol. 4, 1983, p. 13–29.

[4]Miloh, T., "A Note on Three-Dimensional Pursuit Game with Bounded Curvature," *IEEE Transactions on Automatic Control*, Vol. 27, 1982, p. 739–741.

[5]Bryson, A. E., Jr., and Ho, Y. C., *Applied Optimal Control*, Hemisphere, New York, 1975.

[6]Miloh, T., Pachter, M., and Segal, A., "The Effect of a Finite Roll-Rate on the Miss-Distance of a Bank-to-Turn Missile," *Computers and Mathematics with Applications*, Vol. 26, No. 6, 1993, p. 43–54.

[7]Segal, A., and Miloh, T., "A Novel Three-Dimensional Differential Game and Capture Criteria for a Bank-to-Turn Missile," *Journal of Guidance, Control and Dynamics*, Vol. 17, No. 5, 1994, p. 1068–1074.

[8]Segal, A., and Miloh, T., "Barrier Strategies and Capture Criteria in a 3-D Pursuit-Evasion Differential Game," *Optimal Control Applications and Methods*, Vol. 16, 1995, pp. 321–340.

[9]Etkin, B., *Dynamics of Atmospheric Flight*, Wiley, New York, 1972.